Analysis of size-dependent slip transfer and inter-twin flow stress in a nanotwinned fcc metal

Pei Gu [a], Ming Dao [b,*], Subra Suresh [c]

[a] *Department of Engineering Mechanics, Hohai University, Nanjing, Jiangsu 210098, China*
[b] *Department of Materials Science and Engineering, Massachusetts Institute of Technology, Cambridge, MA 02139, USA*
[c] *Department of Materials Science and Engineering, Carnegie Mellon University, Pittsburgh, PA 15213, USA*

Abstract

Nanotwinned structures offer the potential to effectively enhance strength while preserving ductility and damage tolerance. In this paper we present an analytical model for quantifying slip transfer across twin boundaries and for deriving the attendant flow stress as a function of the twin lamellae size in nanotwinned face-centered cubic metals. The mechanistic models investigate how single or piled-up screw and non-screw dislocations interact with twin boundaries, by establishing connections with the size dependence of the activation volume. The models correctly predict the trends from a variety of independent prior experimental observations of the dependence of flow stress on twin lamella size in nanotwinned copper. They also rationalize a number of observations made from previous molecular dynamics simulations of the deformation of nanotwinned metals.
© 2013 Acta Materialia Inc. Published by Elsevier Ltd. All rights reserved.

1. Introduction

The introduction of initially coherent and nanoscale internal interfaces with thermal and mechanical stability offers a means to enhance strength without compromising ductility in metals [1]. An example of such internal interfaces is found in nanoscaled growth twins, typically tens of nanometers in size, embedded within ultrafine grains of several hundred nanometers average size. These nanotwins can be introduced during the processing of metals through such methods as pulsed electrodeposition [1,2]. Nanotwinned polycrystalline metals have been shown to provide high strength while preserving ductility [2–5] as well as damage tolerance during both fracture and fatigue [6,7]. Despite current limitations in the production of

large-volume structural metals and alloys comprising nanotwins, existing reports point to the potential for nanotwinned metals to achieve a more desirable combination of strength, ductility and damage tolerance properties compared to nanograined metals or traditional microcrystalline alloys consisting of microscale twins [1–9].

Asaro and Suresh [10] developed a mechanistic model to rationalize the strength and sensitivity of deformation to the rate of loading in nanostructured metals. They postulated that the emission of partial or perfect dislocations from an existing boundary dislocation or a stress concentration such as a crack at the corner of a sliding boundary is a key mechanistic process influencing the overall mechanical properties. This model was applied to rationalize the strength and rate sensitivity of deformation found in experiments on nanocrystalline metals (with average grain size in the sub-100 nm range) and nanotwinned copper [1,3–5,9].

* Corresponding author.
  E-mail address: mingdao@mit.edu (M. Dao).

Mechanistic modeling of nanograins deals with intra-granular dislocation extension [10]. In a further extension of this approach, an analysis [11,12] of flow stress of nano-twinned metals, as a function of both grain size and twin thickness, was developed by incorporating intra-twin dislocation extension. This analysis captured the size dependence of flow stress in the form of a Hall–Petch-type relationship [13,14]. When the flow stress is known, the activation size (or activation volume) can be determined from the following non-homogeneous nucleation model as a function of grain size and twin thickness [11]:

$$r_c = \alpha \frac{G}{\tau} b \left[\ln \left(\frac{r_c}{r_0} \right) + 1 \right]. \qquad (1)$$

Here, G is the shear modulus, b is the magnitude of the Burgers vector, the non-homogeneous nucleation factor $\alpha < \alpha_h$, where $\alpha_h = 0.057$ is the homogeneous nucleation factor, and the activation volume $V = \pi r_c^2 b/2$, where r_c is the activation size and r_0 is the dislocation core cutoff radius. Since the shear flow stress τ is dependent on both grain size and twin thickness, the activation size (activation volume) also bears the same size dependence. The strain-rate sensitivity is then evaluated as a function of characteristic length scale from $m = \sqrt{3}kT/(VM\tau)$, where M is the Taylor factor, k is the Boltzmann constant and T is the absolute temperature. Here the role of the twin thickness as a nanoscale characteristic length is similar to that of the grain size. In Ref. [11], fitting experimental data of the activation volume gives $\alpha = 0.006$ for nanotwinned Cu (nt-Cu). That analysis also shows α as the representation of stress concentration at the nucleation site with respect to far-field stress (flow stress). The above value for α indicates that the stress concentration factor is about

10 (i.e. $\alpha_h/\alpha \approx 9.57$), which suggests that the shear stress at the nucleation site is several times the flow stress.

A number of studies (see Ref. [1] for an overview) have revealed that coherent internal twin boundaries within the crystalline ensemble of Cu serve both as obstacles to dislocation motion (thereby increasing flow stress) and as locations for nucleating and accommodating dislocations (thereby enhancing ductility and facilitating work hardening). In other words, these mechanistic phenomena associated with the interactions of dislocations with nanoscale twin boundaries differ markedly from those of dislocations in nanograined or microtwinned polycrystalline metals (where the character and coherency of the internal boundaries are very different). How dislocations interact with the twin boundaries by extending across the boundary, being absorbed at the boundary or being transmitted across the boundary to the slip plane of the adjacent twin lamella are, therefore, processes that determine the evolution of flow stress. These processes, in turn, strongly depend on the twin thickness (or spacing or twin density within the grain), which provides a characteristic structural length scale. In analytical modeling [15,16] and atomistic simulation [17–20] of cross-slip, the important dependence on the structural size of deformation or activation volume [1,8–12] of nanotwins was not analyzed.

In this paper, we develop an analytical model of slip transfer in nanotwinned face-centered cubic (fcc) metals, i.e. cross-slip to twin boundary and/or adjacent twin lamella. We investigate scenarios entailing the impingement of nanoscale twin boundaries by a single screw/non-screw dislocation and an array of screw/non-screw dislocations (pileup). The inter-twin flow stress for various dislocation reactions at the twin boundaries is obtained
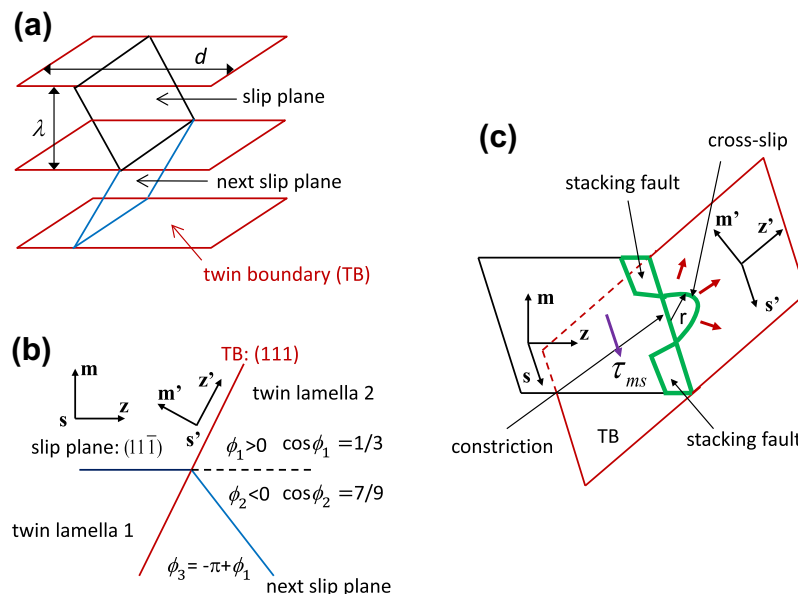

Fig. 1. (a) Schematic representation of the twinned polycrystalline structure in fcc metals showing a twin structure: d, average grain size; λ, twin thickness. (b) Orientation of associated slip planes and the coherent twin boundary. (c) Partials bounded by stacking fault approach twin boundary. They are constricted at the intersection with the twin boundary in activating cross-slip.

by evaluating the free energy change in the activation process of slip transfer. We show that slip transfer in nanoscale twins significantly depends on the twin thickness. The size dependence is explicitly captured in analytical form through the activation volume. The present model thus provides a theoretical approach to evaluate the size-dependent shear stress required for slip transfer at nanoscale twin boundaries.

2. Slip transfer for screw dislocation

2.1. Model for screw dislocation

The coherent twin structure, slip plane orientation and cross-slip process in a nanotwinned fcc metal are schematically illustrated in Fig. 1(a–c); associated slip systems are shown in Fig. 2. In the pileup cross-slip model (Fig. 3(a)), an array of screw dislocations is lined up against the twin boundary; and under external loading, a partial dislocation disassociated from the first screw dislocation is either absorbed onto the twin boundary $\phi = \phi_1$ or transmitted onto the slip plane of the next twin lamella $\phi = \phi_2$ (Fig. 1(b)). At the intersection of the original slip plane with the twin boundary, the two partials which form the screw dislocation **BA** are constricted in order to cross-slip [15,16]. At the initiation of cross-slip, consider a small half-circular partial dislocation loop with radius r moving onto the twin boundary or the slip plane of the adjacent twin lamella from the segment of constriction (Fig. 1(c)). From Refs. [10,11], the energy of the cross-slipped half-circular partial dislocation loop is given as $F_1 = 0.3125 Gb_1^2 r \ln(r/r_0)$, where b_1 is the magnitude of the partial dislocation's Burgers vector. The energy of the initial partial dislocation segment before cross-slip, which corresponds to the half-circular loop after cross-slip, is taken to be the energy per unit length of a straight partial

dislocation scaled by the initial segment length $2r : F_2 = 2r[Gb_1^2 \ln(r/r_0)/(4\pi)]$. Combining the above two expressions, we obtain the energy change due to the lengthening of the loop in the cross-slip process

$$F = F_1 - F_2 = 0.1533 Gb_1^2 r \ln\left(\frac{r}{r_0}\right) \qquad (2)$$

It is noted that rigorous mathematical treatment of the loop energy change, which is complicated and cumbersome, is not sought; the fair approximation here leads to a simple and clear form for inter-twin flow stress with theoretical predictions consistent with experimental data.

The free energy change for the cross-slip of the screw dislocation pileup is [21]

$$\Delta F = \Phi r \ln \frac{r}{r_0} - H\left(r^{\frac{3}{2}} - r_0^{\frac{3}{2}}\right) + P\left(r^2 - r_0^2\right) + 2Ur. \qquad (3)$$

In Eq. (3), the first term on the right side is from the loop energy change in Eq. (2) and $\Phi = 0.1533 Gb_1^2$. In the third term, $P = \pi\Gamma/2$, where $\Gamma = \Gamma_S$ (stacking fault energy) for transmission and $\Gamma = \Gamma_T$ (twin boundary energy) for absorption. In the fourth term, U is the constriction energy. To drive the screw dislocations to enter the twin boundary vicinity, the shear stress τ_{ms} (far-field stress, Fig. 3(a)) acts on the original slip plane with normal **m** (for the **m**–**s**–**z** coordinate system, see Fig. 1(b)) and along the direction of the Burgers vector **BA** shown in Fig. 2. The shear stress to drive the cross-slipped half-circular loop is the near-field stress, given by the mode III crack tip stress field [21],

$$\tau_{m's'} = \frac{K_{III}}{\sqrt{2\pi R}} \cos\left(\frac{\phi}{2}\right), \qquad (4)$$

where $K_{III} = \sqrt{2\pi\lambda}\tau_{ms}$ with λ being the twin thickness; ϕ is the orientation angle and R is the distance along the **z'** axis from the intersection of slip planes (for the **m'**–**s'**–**z'** coordinate system, see Fig. 1(b)). Substituting Eq. (4) into $\tau_{m's'}b_{1s'}$,
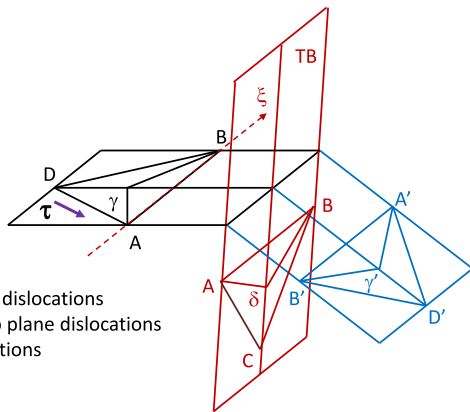

Fig. 2. Perfect and partial dislocation configurations on associated slip planes and the twin boundary. The Burgers vector is defined by the clockwise Burgers circuit when sighting down the positive dislocation line ξ (see Ref. [37]). For screw dislocation **BA**, the reaction at the twin boundary is: γ**A** (leading) + **B**γ (trailing) = γ'**B'** (leading) + **A'**γ' (trailing). For non-screw dislocations **DA** and **AD**, the reactions are as discussed in Section 3.

ABD: slip plane dislocations
A'B'D': next slip plane dislocations
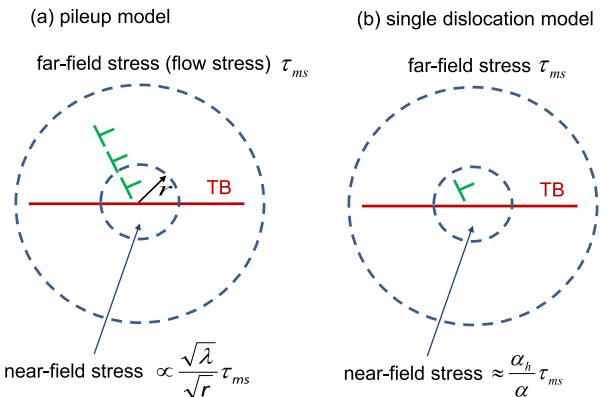ABC: TB dislocations

Fig. 3. Mechanistic models for cross-slip in nanotwins. (a) Pileup dislocation model. The far-field stress is related to the near-field stress by the crack-type stress concentration, $\sim 1/\sqrt{r}$. (b) Single dislocation model. The far-field stress is related to the near-field stress by the ratio of the non-homogeneous nucleation factor α to the homogeneous nucleation factor α_h.

where $b_{1s'} = b_1 \cos 30°$ is the component of the partial's Burgers vector along the **s'** axis, then integrating over the initial half-circular area of cross-slip, we obtain the work done by the shear stress in activation, the second term on the right side of Eq. (3),

$$\int \frac{K_{III}}{\sqrt{2\pi r \sin\theta}} \cos\left(\frac{\phi}{2}\right) b_{1s'} dA$$
$$= 1.4 K_{III} \cos\left(\frac{\phi}{2}\right) b_{1s'}\left(r^{\frac{3}{2}} - r_0^{\frac{3}{2}}\right) = H\left(r^{\frac{3}{2}} - r_0^{\frac{3}{2}}\right), \quad (5)$$

where the area element for the half-circular area is $dA = rdrd\theta$ and $0 \leqslant \theta \leqslant \pi$. The factor on the left side of Eq. (5), $r\sin\theta$, is the distance between the area element and the intersection of slip planes along the **z'** axis. From Eq. (5), $H = 1.98\sqrt{\pi\lambda}\tau_{ms}b_1 \cos(\phi/2)\cos 30°$.

Considering slip transfer as the non-homogeneous creation of a half-circular loop on the cross-slip plane, the cross-slipped loop activates when the free energy change reaches a maximum at the activation size: $\partial\Delta F/\partial r = 0$ at $r = r_a$. Here r_a is the activation size obtained from activation volume V as $r_a = \sqrt{2V/(\pi b)}$, which depends on both twin thickness and grain size d. Some representative values of the activation volume for nt-Cu, which was characterized in Fig. 7 of Ref. [11], are listed in Table 1. These existing data are for a grain size $d = 500$ nm, but both the flow stress from intra-twin dislocation extensions (intra-twin flow stress) and the activation volume are weakly dependent on the grain size in the case of $d \gg \lambda$, as shown in Ref. [11]. The above maximum condition leads to,

$$\tau = \frac{0.06725 G b_1}{\sqrt{\lambda r_a}\cos(\phi/2)}\left(1 + \frac{1}{2}\ln\frac{r_a}{r_0 e} + \frac{r_a P}{\Phi} + \frac{U}{\Phi}\right). \quad (6)$$

Here $\tau \equiv \tau_{ms}$, the required shear stress for cross-slip which is hereafter referred to as inter-twin flow stress. The absorption flow stress is obtained by taking $\phi = \phi_1$, and the transmission flow stress is obtained by taking $\phi = \phi_2$, in Eq. (6). For absorption, instead of $\phi = \phi_3$, we choose $\phi = \phi_1$, which, according to Eq. (4), has a larger driving force than ϕ_3. In transmission, the second partial follows the first; in absorption, when the first partial is activated, both partials repel each other and move in opposite directions [17,18,22]. The first two terms inside the parentheses in Eq. (6) represent the contribution of the loop energy change to the inter-twin flow stress, whereas the last two terms represent the contribution of the stacking fault energy (or twin boundary energy) and the constriction energy, respectively. Using the values of material parameters given below in Section 2.2, it can be seen that the latter contribution is as important as the former.

In the single dislocation cross-slip model (Fig. 3(b)), the second term on the right side of Eq. (3) is replaced with

$-\pi(\bar{\tau}_{ms}\cos\phi)(b_1\cos 30°)(r^2 - r_0^2)/2$, where $\bar{\tau}_{m's'} = \bar{\tau}_{ms}\cos\phi$ is the shear stress on the cross-slip plane. Since r_a is the required size for nucleation at non-homogeneous sites, the ensuing shear stress $\bar{\tau}_{ms}$, extracted from a procedure similar to that used to obtain Eq. (6), is the near-field stress (see Fig. 3(b)). The far-field stress, i.e. inter-twin stress τ, is the near-field stress $\bar{\tau}_{ms}$ divided by the stress concentration factor, which, according to the analysis at the beginning of the article, is the ratio of the homogeneous nucleation factor to the non-homogeneous nucleation factor (≈ 9.57 for nt-Cu). This procedure gives the inter-twin flow stress for the single dislocation model,

$$\tau = \frac{0.11269 G b_1 \alpha}{r_a \alpha_h \cos(\phi)}\left(1 + \frac{1}{2}\ln\frac{r_a}{r_0 e} + \frac{r_a P}{\Phi} + \frac{U}{\Phi}\right). \quad (7)$$

The size dependence is entered into the single dislocation model through the activation size r_a, whereas the size dependence is entered into the pileup model through both r_a and the crack-like stress concentration of dislocation pileup represented by $1\sqrt{\lambda}$ singularity in Eq. (6). Eqs. (6) and (7) show that, similar to intra-twin flow stress discussed in Ref. [11], the inter-twin flow stress is linearly related to the shear modulus and stacking fault energy (or twin boundary energy). In addition, the inter-twin flow stress is linearly related to the constriction energy.

2.2. Prediction for screw dislocation

The material properties of nt-Cu used for the prediction are $G = 50$ GPa, $b = 0.255$ nm and $\Gamma_S/(Gb) = 0.00425$. In the numerical calculation, the twin boundary energy
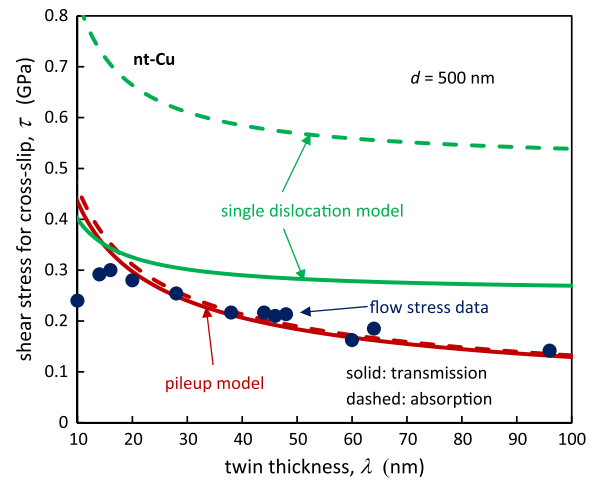

Fig. 4. The shear stress required for the cross-slip of a screw dislocation (inter-twin flow stress) is size-dependent. The single dislocation model requires a higher inter-twin flow stress than the pileup model since the pileup has higher near-field stress. Also plotted are the measured flow stress data of nanotwins in Ref. [2]. At the level of flow stress, both inter- and intra-twin dislocation activities are expected. In the online version, the pileup model (Eq. (6)) is plotted in red lines and the single dislocation model (Eq. (7)) is plotted in green lines, where dashed lines represent absorption and solid lines represent transmission. (For interpretation of the references to colour in this figure legend, the reader is referred to the web version of this article.)

Table 1
Twin-thickness-dependent activation volume (size) of nt-Cu.

$\lambda^{-0.5}$ (nm$^{-0.5}$)	0.1	0.15	0.2	0.25	0.3
$1/V$ (b^{-3})	0.0374	0.0454	0.0607	0.0827	0.1231
r_a (b)	4.1257	3.7446	3.2385	2.7745	2.2741

$\Gamma_T = 0.5\Gamma_S$ [23] and the constriction energy $U = 0.13$ eV/b [24]. The core cutoff radius is taken to be the magnitude of the partial dislocation's Burgers vector, $b_1 = b/\sqrt{3}$.

Fig. 4 shows the inter-twin flow stress predicted by the pileup model and the single dislocation model for screw dislocation. In Fig. 4, the curves for the pileup dislocation model are plotted using Eq. (6); the curves for the single dislocation model are plotted using Eq. (7). Here, dashed lines are for absorption, $\phi = \phi_1$, whereas the solid lines are for transmission, $\phi = \phi_2$. The flow stress for absorption is close to the flow stress for transmission in the pileup model, whereas the former is significantly larger than the latter in the single dislocation model. This distinction arises because the driving force term in the single dislocation model is proportional to $\cos\phi$ such that the driving force for absorption is much smaller than that for transmission. For other nano-twinned materials (such as aluminum), atomistic simulation shows absorption also occurs [20]. In Fig. 4, the predicted order of magnitude for inter-twin flow stress and the predicted behavior for transmission vs. absorption are consistent with those found in molecular dynamics (MD) simulation [17], which was performed under similar external loading and which showed that **BA** is transmitted to γ'**B** + **A**γ'. Experimental data of flow stress for nt-Cu [2] as a function of the characteristic structural length (twin thickness), λ, are also given in the figure. Comparing these data with the predictions of the inter-twin flow stress here and the intra-twin flow stress given in Ref. [11], we observe that both inter- and intra-twin dislocation activities are expected when loading reaches the flow stress level in nt-Cu. The inter-twin flow stress τ we obtained through Eqs. (6) and (7) is the theoretically predicted critical resolved shear stress.

From Eq. (6), the criterion for transmission in the pileup model is

$$\frac{\left(1 + \frac{1}{2}\ln\frac{r_a}{r_0 e} + \frac{\pi r_a \Gamma_S}{2\Phi} + \frac{U}{\Phi}\right)\cos\frac{\phi_1}{2}}{\left(1 + \frac{1}{2}\ln\frac{r_a}{r_0 e} + \frac{\pi r_a \Gamma_T}{2\Phi} + \frac{U}{\Phi}\right)\cos\frac{\phi_2}{2}} < 1. \tag{8}$$

The criterion for absorption is to replace the sign "<" by ">" in Eq. (8). For the single dislocation model, the criterion is written by replacing $\phi_1/2$ and $\phi_2/2$ with ϕ_1 and ϕ_2, respectively, where these angles come from the orientation-dependent driving force such as Eq. (4). For the pileup model, the ratio on the left side is close to one, as seen in Fig. 4.

The typical free energy path, i.e. the free energy change vs. the cross-slipped half-circular loop size, is shown in Fig. 5. The activation energy shown in the figure falls into the range obtained from atomistic simulation [18]. For the single dislocation model, cross-slip needs to overcome a steeper energy barrier to acquire the required activation energy. In reality, the activation energy for the pileup case is expected to be higher than predicted because of the idealization of crack-like singularity for an array of dislocations. In general, the constriction energy in Eq. (3) should include a point constriction energy term U_0, i.e. $2rU + U_0$ [16]. The constant term for point constriction does not alter the
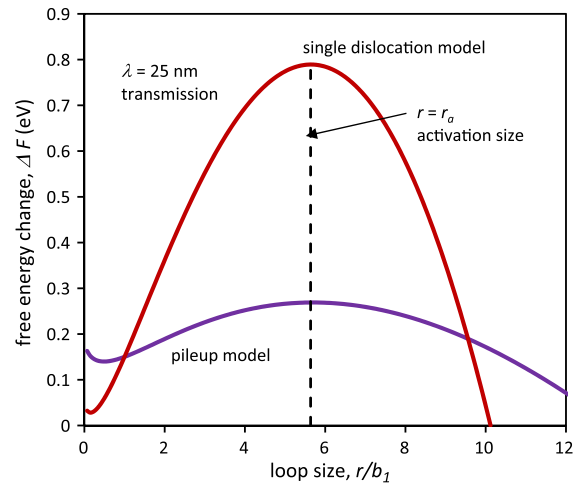

Fig. 5. Typical free energy path for cross-slip at a nanotwin boundary. The figure illustrates that cross-slip in nanotwins requires sufficient activation energy to expand the loop in the cross-slip plane; the activation size is several times the Burgers vector of the partial dislocations. The energy barrier for the pileup model is lower than that for the single dislocation model.

inter-twin flow stress, which is obtained in maximizing the free energy change (taking derivative) of Eq. (3). For the free energy path in Fig. 5, a large value of U_0 shifts the two curves up, but does not change the difference of them.

For very small twin thicknesses (<15 nm), strength softening (see Refs. [2,12]) occurs such that the trend of theoretical prediction becomes different from the experimental data (the far left side of Fig. 4). Strength softening at very small twin thicknesses may be caused by the nucleation of dislocations on the twin boundary [25], a different deformation mechanism.

3. Slip transfer for non-screw dislocation

3.1. Model for non-screw dislocation

Obeying the conservation of Burgers vectors [26], the cross-slip of non-screw dislocations to a twin boundary and/or the next twin lamella is possible. The reactions for 60° dislocation at the twin boundary have been discussed previously in MD simulation [27]. For nt-Cu, MD shows that the non-screw dislocation **DA** (=γ**A** (leading) + **D**γ (trailing)) under shear stress acting along the dislocation's Burgers vector is transferred to one 90° twinning partial, **C**δ, and two partials on the next slip plane, γ**D'** (leading) + **A'**γ' (trailing) (see Fig. 2). For the case of reverse dislocation **AD** (=γ**D** (leading) + **A**γ (trailing)), the reaction with the twin boundary results in a 30° partial γ'**A'** on the next slip plane and a Hirth lock (1/3[0 0 1]; see Ref. [28])[1] with a mismatch (1/9[1 1 1]) at the intersection.

---

[1] The Hirth lock is a sessile dislocation which results from the reaction of two partials at the intersection of slip planes, similar to the manner in which a Lomer–Cottrell lock forms. An example of the partial dislocation reaction that produces a Hirth lock is: $1/6[\bar{2}11] + 1/6[2\bar{1}1] = 1/3[001]$ (see Ref. [28]).

Since the two partials on the original slip plane are recombined before cross-slip, it can be easily seen that the energy criterion (Frank rule) in the above two reactions for non-screw dislocations is not violated. We evaluate the inter-twin flow stress for non-screw dislocations **DA** and **AD** by generalizing the approach for screw dislocation in the previous section.

For **DA**, the required shear stress for cross-slip activates the partial **Cδ** on the twin boundary and the leading partial γ**'D'** on the slip plane of adjacent twin lamella. The shear stresses on the respective slip planes to drive the two partials are those along the Burgers vectors of the two 90° partials, resolved from $\tau_{mz} = \tau \cos 30^\circ = \sqrt{3}\tau/2$ on the original slip plane, where τ, as shown in Fig. 2, is along the direction of **DA**. For the pileup model, these shear stresses for cross-slip are the near-field stresses, calculated from the mode II crack tip stress field [21,29],

$$\tau_{m'z'} = \frac{K_{II}}{\sqrt{2\pi R}}\left[\frac{1}{4}\cos\left(\frac{\phi}{2}\right) + \left(\frac{3}{4}\right)\cos\left(\frac{3\phi}{2}\right)\right], \quad (9)$$

where $K_{II} = \sqrt{2\pi\lambda}\tau_{mz}$. Taking the orientation angles for absorption and transmission (Fig. 1(b)), we obtain, from Eq. (9), the shear stress along **Cδ**, $\tau_T = K_{II}/\sqrt{2\pi r}/\sqrt{3}$; the shear stress along γ**'D'**, $\tau_S = 4\sqrt{2}K_{II}/\sqrt{2\pi r}/9$. The work done by the external loading is the integration of $\tau_T b_1 + \tau_S b_1$ over the initialized half-circular area of cross-slip on both slip planes, such that the free energy change is

$$\Delta F = 2\Phi r\ln\frac{r}{r_0} - H^*\left(r^{\frac{3}{2}} - r_0^{\frac{3}{2}}\right) + P^*(r^2 - r_0^2) + 2Ur. \quad (10)$$

Here, $H^* = 2.068\sqrt{\pi\lambda}\tau b_1$ and $P^* = \pi(\Gamma_S + \Gamma_T)/2$. Eq. (10) is similar to Eq. (3) in Section 2 for the pileup model of screw dislocation, but here two half-circular loops on two cross-slip planes, one for **Cδ** and another for γ**'D'**, are evaluated. Maximizing ΔF in Eq. (10) with respect to r at the activation size r_a leads to the inter-twin flow stress for **DA**,

$$\tau = \frac{0.1115Gb_1}{\sqrt{\lambda r_a}}\left(1 + \frac{1}{2}\ln\frac{r_a}{r_0 e} + \frac{r_a P^*}{2\Phi} + \frac{U}{2\Phi}\right). \quad (11)$$

For **AD** in the pileup model, the Hirth lock and mismatch are sessile and thus inactive during the cross-slip, and the cross-slip of the partial γ**'A'** shown in Fig. 2 activates the slip transfer process. In this case, the shear stress τ on the original slip plane is along the direction of **AD**. To calculate the work done by shear stress on the cross-slipped half-circular loop, the partial and shear stress on the next slip plane are projected to the two perpendicular directions, **A'B'** and γ**'D'**, to calculate the work done along these two directions separately; these are then summed up. It is seen that the model III crack tip stress field drives the dislocation component along the direction of **A'B'**, whereas the model II crack tip stress field drives the dislocation component along the direction of γ**'D'**. From Eq. (4), the shear stress along the direction of **A'B'** is $\tau_{S1} = 2\sqrt{2}K_{III}/\sqrt{2\pi r}/3$, where $K_{III} = -\sqrt{2\pi\lambda}\tau/2$. From Eq. (9), the shear stress along the direction of γ**'D'** is $\tau_{S2} = 4\sqrt{2}K_{II}/\sqrt{2\pi r}/9$, where $K_{II} = -\sqrt{2\pi\lambda}(\sqrt{3}/2)\tau$. The Burgers vector's components

of the partial γ**'A'** along the directions of **A'B'** and γ**'D'** are $-\sqrt{3}b_1/2$ and $-b_1/2$, respectively. Thus, the work done by the external loading in activation is the integration of $-\sqrt{3}\tau_{S1}b_1/2 - \tau_{S2}b_1/2$ over the initialized half-circular area of cross-slip. In this case, the free energy is in the same form as that in Eq. (3), but with different H. Evaluating the work done by external loading, we obtain $H = 1.347\sqrt{\pi\lambda}\tau b_1$. The inter-twin flow stress for the non-screw dislocation **AD** is then obtained by maximizing the free energy change,

$$\tau = \frac{0.0855Gb_1}{\sqrt{\lambda r_a}}\left(1 + \frac{1}{2}\ln\frac{r_a}{r_0 e} + \frac{r_a P_1}{\Phi} + \frac{U}{\Phi}\right). \quad (12)$$

Here, $P_1 = \pi\Gamma_S/2$.

The approach for the single non-screw dislocation is similar to that in Section 2 for the single screw dislocation, evaluating resolved shear stresses on the cross-slip planes based on the shear stress on the original slip plane. The mathematical steps are given in Appendix A. The resulting inter-twin flow stresses are

$$\tau = \frac{0.2282Gb_1\alpha}{r_a\alpha_h}\left(1 + \frac{1}{2}\ln\frac{r_a}{r_0 e} + \frac{r_a P^*}{2\Phi} + \frac{U}{2\Phi}\right), \quad (13)$$

for dislocation **DA** and

$$\tau = \frac{0.2282Gb_1\alpha}{r_a\alpha_h}\left(1 + \frac{1}{2}\ln\frac{r_a}{r_0 e} + \frac{r_a P_1}{\Phi} + \frac{U}{\Phi}\right), \quad (14)$$

for dislocation **AD**.

For **AD**, the sessile dislocations left at the twin boundary can block subsequent incoming dislocations. The associated dislocation accumulation near the twin boundary will lead to strain hardening, while further reactions are needed for incoming dislocations and sessile dislocations to initiate any subsequent slip transfers. For **DA** and screw dislocations, because there are no sessile dislocations left at the twin boundary, more slip transfers through the same reactions discussed earlier are favorably expected. This fact suggests that different characters of dislocations at the twin boundary may result in different deformation behaviors.

The above discussion for screw and non-screw dislocations focuses on nt-Cu. For the other nanotwinned fcc materials, dislocations at the twin boundary can exhibit different reactions, as shown by MD simulations in Refs. [17,27]. Furthermore, there have been no data for twin-thickness-dependent activation size r_a for nanotwinned materials other than nt-Cu. Future studies of slip transfer in other nanotwinned metals could be carried out based on the analytical approach discussed here when the data of twin-thickness-dependent activation size for these materials become available.

3.2. Prediction for non-screw dislocation

Fig. 6 is a plot of the inter-twin flow stress predicted by the single dislocation model and pileup model for **DA** and **AD**. The pileup dislocation model and single dislocation model for **DA** are plotted in dashed lines using Eqs. (11) and (13), respectively; the pileup dislocation model and
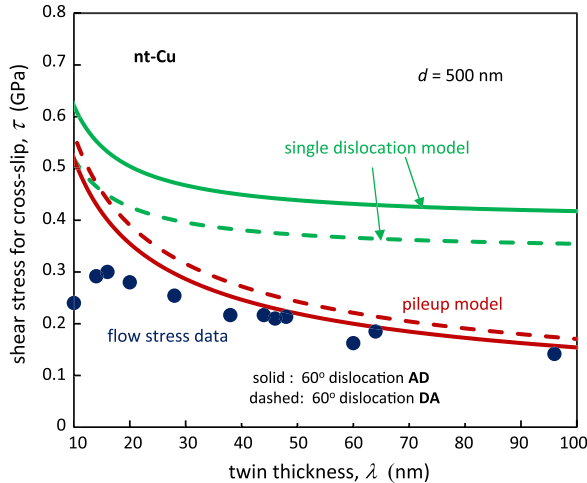
Fig. 6. The shear stress required for cross-slip of non-screw dislocation (inter-twin flow stress) is size-dependent and higher than that of screw dislocation. The required shear stress for the 60° dislocation **AD** is different from that for **DA** because their reactions with the twin boundary are different. Also plotted are the measured flow stress data of nanotwins in Ref. [2]. In the online version, the pileup model is plotted in red lines for **DA** (Eq. (11)) and **AD** (Eq. (12)); the single dislocation model is plotted in green lines for **DA** (Eq. (13)) and **AD** (Eq. (14)). (For interpretation of the references to colour in this figure legend, the reader is referred to the web version of this article.)

single dislocation model for **AD** are plotted in solid lines using Eqs. (12) and (14), respectively. Compared to the inter-twin flow stress obtained for the screw dislocation in Fig. 4, this figure shows that the shear stress required for cross-slip of a non-screw dislocation is higher than that for a screw dislocation. This is consistent with the fact that the crystallographic nature of screw dislocations is more favorable for slip transfer. Despite this, the inter-twin flow stresses in Figs. 4 and 6 are of the same order of magnitude, and are within a comparable range to the flow stress data. As in Fig. 4, for very small twin thicknesses (<15 nm), the trend of the theoretical prediction on the far left side of Fig. 6 becomes different from the experimental data because the strength softening at very small twin thicknesses is caused by mechanisms other than slip transfer induced strengthening. For the single dislocation model, the magnitude of the inter-twin flow stress in Fig. 6 appears to be smaller than the prediction from MD simulation [27], and this may be due to the higher strain rate imposed in the MD simulation. In addition, the constriction energy used in our calculation for the non-screw dislocation case is the one obtained for screw dislocation [24]. A simple estimate in Appendix B shows that the constriction energy for a non-screw dislocation can be much higher than that for a screw dislocation. In view of these factors, our predictions are consistent with the flow stress data [2] and MD simulation results for screw and non-screw dislocations [17,18,27].

4. Concluding remarks

The current study considers the interactions of either a dislocation pileup or a single dislocation with a twin

boundary. When initial dislocations are away from the twin boundary area, additional stress is needed to push them into the vicinity of the twin boundary to overcome the long-range repulsive force [30]. As the transmitted dislocation loop extends extensively across the slip plane of adjacent twin lamella, dislocation glide in the nanotwin would eventually be governed by the intra-twin flow stress model [11]. For twins in microcrystalline materials [31], their size dependence for slip transfer does not appear to be as important as that found in nanotwins, since the activation volume for microcrystalline materials is much larger than that for nanocrystalline and nanotwinned materials such that microtwins exhibit much smaller strain-rate sensitivity, as seen in Refs. [10,11,32].

For a single crystalline nanotwinned copper with only one twin system, our theoretical framework naturally contains the load orientation dependence through the resolved shear stress. The inter-twin flow stress τ we obtained in Eqs. (6), (7), (11)–(14) is the theoretically predicted critical resolved shear stress for each case. For a general applied load represented by stress tensor **T**, the critical condition for slip transfer may be written as $\mathbf{m} \cdot \mathbf{T} \cdot \mathbf{b}/|\mathbf{b}| = \tau$, where **m** is the unit normal of the original slip plane and **b** is the Burgers vector. In the results shown in Figs. 4 and 6, we compare the analytical results with the size-dependent experimental results performed using random-textured nanotwinned copper samples. These samples have a macroscopically isotropic plastic behavior due to the random texture. A standard Taylor factor ($M = 3$) is taken for the polycrystalline random-textured nanotwinned copper to correlate the macroscopic yield strength with the resolve shear stress at the single crystal level. For the polycrystalline nanotwinned copper that has a strong texture (e.g. columnar-grained nanotwinned copper [33]), depending on the externally applied stress state, both the inter-twin flow stress studied here and the intra-twin flow stress studied in Ref. [11] are expected to contribute to the plastic flow, while their respective contributions are strongly orientation dependent. The detailed analyses involving both inter- and intra-twin dislocation activities are suggested in a future effort using the presented theoretical framework.

In this paper, we have described a mechanistic model for the slip transfer of dislocations in nt-Cu. The size-dependent slip transfer process is introduced into the present model through a size-dependent activation volume. The model is shown to correctly predict the dependence of flow stress of nt-Cu on the nanotwin lamella size. When the activation volumes of other fcc metals containing nanotwins become available, the present analysis can be applied to examine various other dislocation reactions [27,34] occurring at twin boundaries and their consequences for deformation and strain hardening. Such future studies could also address the size dependence of slip transfer in other twinned crystal structures, e.g. body-centered cubic and hexagonal close-packed metals [35], and in other types of twinning, such as deformation twins [35,36].

Acknowledgements

Appendix A. Model for single non-screw dislocation

For the single non-screw dislocation **DA** shown in Fig. 2, the free energy expression is the same as Eq. (10), but with a different driving force term (the second term on the right side). To obtain this driving force term, we evaluate the resolved shear stresses along γ'**D**' on the next slip plane and **Cδ** on the twin boundary, from the shear stress acting along the Burgers vector **DA** on the original slip plane τ. The shear stress acting on γ'**D**' is $\tau_S = 17\sqrt{3}\tau/162$ and the shear stress acting on **Cδ** is $\tau_T = 7\sqrt{3}\tau/18$. The work by the external loading W in activation is the integration of $(\tau_S + \tau_T)b_1\alpha_h/\alpha$ (the factor α_h/α denotes the stress concentration at non-homogeneous nucleation site as discussed in Section 2) over the initialized half-circular area of cross-slip,

$$W = \frac{\pi}{2}\left(\frac{7\sqrt{3}}{18} + \frac{17\sqrt{3}}{162}\right)\frac{b_1\alpha_h\tau}{\alpha}(r^2 - r_0^2). \quad (A1)$$

Replacing the second term on the right side of Eq. (10) by the above expression and maximizing the free energy change at the activation size r_a, we obtain the inter-twin flow stress in Eq. (13).

For single non-screw dislocation **AD**, the free energy expression is the same as Eq. (3), but with a different driving force term (the second term on the right side). To obtain this driving force term, we evaluate the resolved shear stresses along **A**'**B**' and γ'**D**' on the next slip plane from the shear stress acting along the Burgers vector **AD** on the original slip plane τ. The shear stress along the direction of **A**'**B**' on the next slip plane is $\tau_{S1} = -7/18\tau$, and the shear stress along the direction γ'**D**' on the next slip plane is $\tau_{S2} = -17\sqrt{3}\tau/162$. The Burgers vector's components of the partial γ'**A**' along the directions **A**'**B**' and γ'**D**' are $-\sqrt{3}b_1/2$ and $-b_1/2$, respectively. So, the work by the external loading W in activation, considering stress concentration at the nonhomogeneous nucleation site α_h/α, is the integration of $(-\sqrt{3}\tau_{S1}b_1/2 - \tau_{S2}b_1/2)\alpha_h/\alpha$ over the initialized half circular area of cross-slip,

$$W = \frac{\pi}{2}\left(\frac{7\sqrt{3}}{36} + \frac{17\sqrt{3}}{324}\right)\frac{b_1\alpha_h\tau}{\alpha}(r^2 - r_0^2). \quad (A2)$$

Replacing the second term on the right side of Eq. (3) by the above expression and maximizing the free energy change at the activation size r_a, we obtain the inter-twin flow stress in Eq. (14).

Appendix B. Estimation of constriction energy

We estimate the constriction energy from dislocation theory. According to Ref. [38], for a straight dislocation, the energy change for the leading partial to extend a distance δ is

$$\Delta E = -2E_{12}\ln\frac{\delta}{r_0} + \Gamma_S(\delta - r_0). \quad (A3)$$

Here, $E_{12} = K_{ij}b_{1i}b_{2j}$. For the coordinate system on the original slip plane shown in Fig. 1 (formed by the indicated axes **m**, **s** and **z**), the dislocation line is parallel to the **s** axis; the coefficient $K_{mm} = K_{zz} = G/(4\pi(1 - v))$, with v being Poisson's ratio; $K_{ss} = 1/(4\pi)$; and $K_{ij} = 0$ for $i \neq j$. b_{1i} and b_{2i} ($i = 1,2,3$) are the projections of the leading and trailing partials' Burgers vectors onto the **m**–**s**–**z** axes, respectively. The equilibrium distance of the leading and trailing partials, d_0, is obtained from $\partial\Delta E/\partial\delta = 0$, which gives

$$d_0 = \frac{2E_{12}}{\Gamma_S}. \quad (A4)$$

Considering that the separation of the two partials is constricted to d from d_0, the energy change required for this process is

$$\Delta E_1 = -2E_{12}\ln\frac{d}{d_0} + \Gamma_S(d - d_0). \quad (A5)$$

Using the relation $\Gamma_S = 2E_{12}/d_0$. from Eq. (A4), Eq. (A5) is rewritten as

$$\Delta E_1 = -2E_{12}\left(\ln\frac{d}{d_0} - \frac{d}{d_0} + 1\right). \quad (A6)$$

Eq. (A6) is similar to that used for discussion in Ref. [24]. From Eq. (A6), the larger the coefficient E_{12}, the larger the constriction energy. We compute E_{12} for the screw dislocation **BA** and non-screw dislocation **DA** in Fig. 2. In the **m**–**s**–**z** coordinate system, for **BA**, $\mathbf{b}_1 = \mathbf{B}\gamma = \lfloor 0, b/2, -b/(2\sqrt{3})\rfloor$ and $\mathbf{b}_2 = \gamma\mathbf{A} = \lfloor 0, b/2, b/(2\sqrt{3})\rfloor$, which gives $E_{12} = Gb^2/(32\pi)$ (with the Poisson's ratio taken as $v = 1/3$). For **DA**, $\mathbf{b}_1 = \mathbf{D}\gamma = \lfloor 0, 0, b/\sqrt{3}\rfloor$ and $\mathbf{b}_2 = \gamma\mathbf{A} = \lfloor 0, b/2, b/(2\sqrt{3})\rfloor$, which gives $E_{12} = Gb^2/(16\pi)$. The above two values for E_{12} suggest that the constriction energy for non-screw dislocation can be much larger than that for screw dislocation.

References

[1] Lu K, Lu L, Suresh S. Science 2009;324(5925):349–52.
[2] Lu L, Chen X, Huang X, Lu K. Science 2009;323(5914):607–10.
[3] Lu L, Schwaiger R, Shan ZW, Dao M, Lu K, Suresh S. Acta Mater 2005;53(7):2169–79.
[4] Lu L, Zhu T, Shen YF, Dao M, Lu K, Suresh S. Acta Mater 2009;57(17):5165–73.
[5] Dao M, Lu L, Shen YF, Suresh S. Acta Mater 2006;54(20):5421–32.
[6] Singh A, Dao M, Lu L, Suresh S. Acta Mater 2011;59(19):7311–24.
[7] Singh A, Tang L, Dao M, Lu L, Suresh S. Acta Mater 2011;59(6):2437–46.
[8] Lu L, Dao M, Zhu T, Li J. Scripta Mater 2009;60(12):1062–6.

[9] Dao M, Lu L, Asaro RJ, De Hosson JTM, Ma E. Acta Mater 2007;55(12):4041–65.

[10] Asaro RJ, Suresh S. Acta Mater 2005;53(12):3369–82.

[11] Gu P, Dao M, Asaro RJ, Suresh S. Acta Mater 2011;59(18):6861–8.

[12] Gu P, Dao M. Appl Phys Lett 2013;102(9):091904.

[13] Hall EO. Proc Phys Soc London, Sect B 1951;64(381):747–53.

[14] Petch NJ. J Iron Steel Inst, London 1953;174(1):25–8.

[15] Escaig B. In: Rosenfield AR, Hahn GT, Bement AL, Jafee RI, editors. Dislocation dynamics. New York: McGraw-Hill; 1968.

[16] Puschl W. Prog Mater Sci 2002;47(4):415–61.

[17] Jin ZH, Gumbsch P, Ma E, Albe K, Lu K, Hahn H, et al. Scripta Mater 2006;54(6):1163–8.

[18] Zhu T, Li J, Samanta A, Kim HG, Suresh S. Proc Natl Acad Sci USA 2007;104(9):3031–6.

[19] Kulkarni Y, Asaro RJ. Acta Mater 2009;57(16):4835–44.

[20] Dewald MP, Curtin WA. Philos Mag 2007;87(30):4615–41.

[21] Asaro RJ, Rice JR. J Mech Phys Solids 1977;25(5):309–38.

[22] Asaro RJ, Kulkarni Y. Scripta Mater 2008;58(5):389–92.

[23] Zhu YT, Liao XZ, Srinivasan SG, Zhao YH, Baskes MI, Zhou F, et al. Appl Phys Lett 2004;85(21):5049–51.

[24] Rasmussen T, Jacobsen KW, Leffers T, Pedersen OB, Srinivasan SG, Jonsson H. Phys Rev Lett 1997;79(19):3676–9.

[25] Li XY, Wei YJ, Lu L, Lu K, Gao HJ. Nature 2010;464(7290):877–80.

[26] Sutton P, Balluffi RW. Interfaces in crystalline materials. Oxford: Oxford University Press; 1995.

[27] Jin ZH, Gumbsch P, Albe K, Ma E, Lu K, Gleiter H, et al. Acta Mater 2008;56(5):1126–35.

[28] Hirth JP, Lothe J. Theory of dislocations. 2nd ed. New York: Wiley; 1982.

[29] Anderson TL. Fracture mechanics – fundamentals and applications. Boca Raton, FL: CRC Press; 1995.

[30] Chen ZM, Jin ZH, Gao HJ. Phys Rev B 2007;75(21):212104.

[31] Clark WAT, Wagoner RH, Shen ZY, Lee TC, Robertson IM, Birnbaum HK. Scripta Metall Mater 1992;26(2):203–6.

[32] Armstrong RW. Emerg Mater Res 2012;1(Sp.1):31–7.

[33] You ZS, Li XY, Gui LJ, Lu QH, Zhu T, Gao HJ, et al. Acta Mater 2013;61(1):217–27.

[34] Zhu YT, Wu XL, Liao XZ, Narayan J, Kecskes LJ, Mathaudhu SN. Acta Mater 2011;59(2):812–21.

[35] Christian JW, Mahajan S. Prog Mater Sci 1995;39(1–2):1–157.

[36] Mahajan S. Scripta Mater 2013;68(2):95–9.

[37] Weertman J, Weertman JR. Elementary dislocation theory. New York: Oxford University Press; 1992.

[38] Asaro RJ, Krysl P, Kad B. Philos Mag Lett 2003;83(12):733–43.